Composite biomaterials as long-lasting scaffolds for 3D bioprinting of highly aligned muscle tissue

A. García-Lizarribar[1,2,a], Xiomara Fernández Garibay[1,a], Ferran Velasco Mallorquí[1], Albert Garcia Castaño[1], Josep Samitier[1,2,3,], Javier Ramon-Azcon[1,*]*

[1]Institute for Bioengineering of Catalonia (IBEC), The Barcelona Institute of Science and Technology, Baldiri Reixac 10-12, 08028 Barcelona Spain

[2]Centro de Investigación Biomédica en Red (CIBER), Madrid 28029, Spain

[3]Department of Electronic and Biomedical Engineering, University of Barcelona (UB), Barcelona 08028, Spain

[1] García-Lizarribar, Xiomara Fernández Garibay, Ferran Velasco Mallorquí, Dr. Albert Garcia Castaño, Prof. Josep Samitier, Dr. Javier Ramon-Azcon
Institute for Bioengineering of Catalonia (IBEC), The Barcelona Institute of Science and Technology, Baldiri Reixac 10-12, 08028 Barcelona Spain
E-mail: jramon@ibecbarcelona.eu; E-mail: jsamitier@ibecbarcelona.eu

[2] García-Lizarribar, Prof. Josep Samitier
Centro de Investigación Biomédica en Red (CIBER), Madrid 28029, Spain

[3] Prof. Josep Samitier
Department of Electronic and Biomedical Engineering, University of Barcelona (UB), Barcelona 08028, Spain

[a] These authors contributed equally to this work

* Corresponding authors

ABSTRACT

New biocompatible materials have enabled the direct 3D printing of complexes functional living tissues, such skeletal and cardiac muscle. Gelatin-methacryloyl (GelMA) is a photopolymerizable hydrogel composed of natural gelatin functionalized with methacrylic anhydride. However, it is difficult to obtain a single hydrogel that meets all desirable properties. In particular, GelMA hydrogel lacks versatility in their mechanical properties and lasting 3D structures. In this work, we present a library of composite biomaterials to obtain versatile, lasting and mechanically tunable scaffolds. We combined two polysaccharides, alginate (Alg) and carboxymethyl cellulose (CMC) chemically functionalized with methacrylic anhydride, and a synthetic material, such as poly(ethylene glycol) diacrylate (PEGDA) with GelMA to obtain photopolymerizable hydrogel blends. We screened and optimized the physical properties of the obtained composite hydrogels for the growth and development of skeletal muscle fibers from C2C12 murine cells and we compare the results with pristine GelMA. All these composites show high resistance to the degradation capability maintaining with high fidelity the 3D structure over several weeks. Altogether, in this study we develop and characterize a library of biocompatible novel and totally versatile composite biomaterials with tunable mechanical properties that give structure and support myotube formation and alignment.

1. INTRODUCTION

Engineered muscle tissues (skeletal and cardiac muscle) have *in vivo* regenerative medicine applications that involve harvesting cells from the patient, growing them within a suitable scaffolding material, and reintroducing them into the patient [1-3]. Moreover, these engineered tissues also have *in vitro* applications such as drug screening, bio-actuators and biosensors [4-8]. Especially interesting is the use of engineered muscle tissues as bio-actuators. Intrinsically bio-compatible materials, such tissues can be integrated in biomedical devices to harvest energy and produce micro controlled actuators. Specific examples include the application of skeletal muscle tissue on a Si-MEMS device to act as a micro bio-actuator for energy harvesting [9], bio-actuators operated by self-assembled insect muscle tissue [10], or integration of optogenetic myotubes with MEMS systems [11]. In all of these systems, the contractile ability of muscle tissue is needed and can only be obtained with a correct microarchitecture of the tissue, superior adaptable mechanical properties of the material where the tissue is attached, and a stable 3D structure. Important advances have been made in this area, but one of the major obstacles in engineering 3D complex tissues such as muscle is the need to encapsulate the cells in a long-lasting biocompatible 3D environment with adaptable mechanical properties [12]. To date, many technologies, including photolithography, electrospinning and bioprinting [12-16], have been adopted for the fabrication of 3D tissue constructs. Among them, bioprinting shows exciting potential as it is able to provide precise spatial manipulation of living cells with a suitable 3D growth environment, optimal oxygen levels and effective nutrient transport, as well as mechanical integrity.

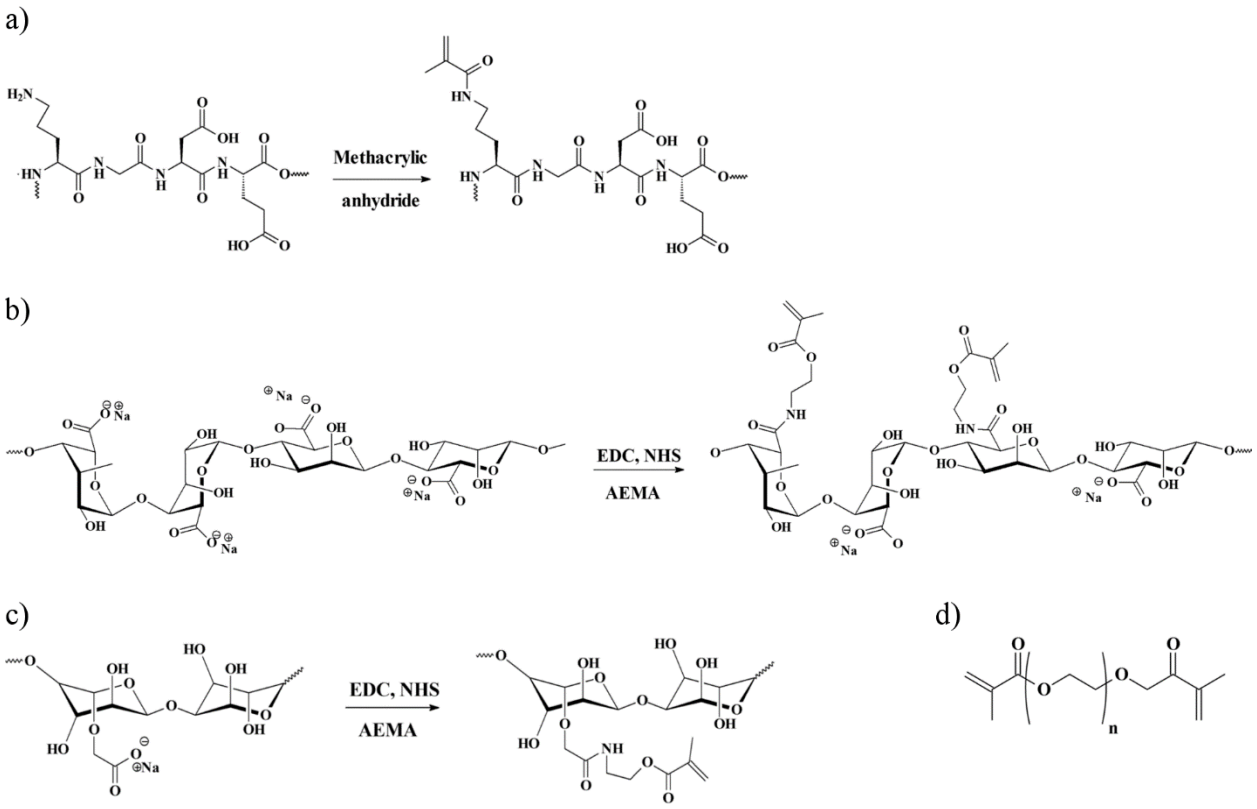

Figure 1. Covalent functionalization of the photocrosslinkable materials, a) methacryloylated gelatin (GelMA), b) Alginate-methacrylat (AlgMA), c) Microfibrillated cellulose-methacrylat (CMCMA), and d) PEGDA.

Cell responsive bioinks are a critical component in bioprinting technology. Hydrogel-based bioinks encapsulating living cells and bioactive components are commonly used for bioprinting. Currently, natural materials derived from mammalian animals (e.g. collagen, gelatin and fibrin) are more suitable for engineering skeletal muscle due to higher cell attachment density, greater rates of cell proliferation, gel compaction (resulting in greater final cell density), and endogenous provision of growth factors and biological signals for differentiation [17, 18]. So far, a range of natural hydrogels including gels such as collagen/gelatin [19], gelatin-methacryloyl (GelMA) [20, 21], alginate [22], fibrin [23] and hyaluronic acid (HA) [24] have been used in bioprinting, but none of

these materials have been able to fulfil all the requirements necessary for engineering muscle tissue bioactuators, such as mechanical properties, and formation of stable and durable structures. These 3D natural scaffolds are degraded by mammalian cells and the structural functionality of the bioactuator finally is lost [25].

To overcome the lack of 3D geometry along the time and obtain long-lasting architectures, composite materials can be obtained through combination of degradable and non-degradable materials of both synthetic [14, 25-27] and natural [24, 28-31] origin. Among the distinct types of natural non-biodegradable biomaterials, polysaccharides, due to their biocompatibility and chemical properties, have attracted considerable attention in biomedical and pharmaceutical applications [32, 33]. Carboxymethyl cellulose (CMC) is a water-soluble and biocompatible derivative of cellulose and it is derived from abundant renewable resources. CMC hydrogels are not biodegradable by mammalian cells and, for this reason, they can be used as a natural biocompatible material to produce non-degradable structures [34]. Only a few applications use it to encapsulate cells [30, 35] and CMC-methacrylat combined with GelMA has never been tested in tissue engineering applications. Alginate is a more widely used polysaccharide in tissue engineering applications. Alginate is a linear unbranched polysaccharide, derived from seaweed, that contains repeating units of 1,4-linked b-D-mannuronic acid and a-L-guluronic acid. It gels in the presence of divalent cations, such as calcium, barium, and magnesium [36]. Alginate without any modification has been used in combination with GelMA [29], and it has also been methacrylated and used to encapsulate chondrocytes cells [28] . In addition, GelMA and AlgMA have been already combined to encapsulate human osteoblast-like cells (MG63s) and human umbilical cord vein endothelial cells (HUVECs) [37]. Although previous studies have reported promising results, there is still limited control over the mechanical properties, swelling ratios, and the consequent effects on the cell

differentiation process of these polysaccharides and their respective composite biomaterials with GelMA. Finally, PEGDA is one of the most popular synthetic materials used in tissue engineering applications [38], because of its high hydrophilicity, bioinert structure, lack of toxic or immunogenic responses, and cannot degraded by mammalian cells. Also, PEG-based hydrogels provide adjustable mechanical properties as their elastic modulus can be tuned over a broad range of values to mimic the moduli of soft tissues [39]. In bioprinting applications, it has been used in combination with natural hydrogels to produce composite hydrogel formulations [27].

Here, we report evaluation of three photocrosslinkable composite materials (i.e. GelMA-alginate-methacrylat (GelMA-AlgMA), GelMA-carboxymethyl cellulose-methacrylatd (GelMA-CMCMA)) and GelMA-PEGDA, as bioinks for engineering skeletal muscle tissue. Employing GelMA gels in combination with different non-biodegradable materials (i.e. alginate, cellulose and PEGDA), we obtained composite materials for direct bioprinting of 3D cell-laden skeletal muscle constructs with high structural fidelity, enhanced bioactivity, and long-standing structures. We formulated a library of composite hydrogel prepolymer solutions with different prepolymers concentrations, UV dosage and two different UV photoinitiators. Photopolymerizable hydrogels show a close relationship between their mechanical properties and their crosslinking density [40, 41] and stiffness of hydrogels strongly affects cell behavior and can induce or inhibit cell differentiation towards different phenotypes [39, 42-44]. We tuned the mechanical properties of the resulting hydrogels by varying the time of UV-induced crosslinking and photoinitiator concentration. We hypothesized that pore size frequency distribution have also significant impact on cell behavior [31]. The diffusion of nutrients inside the structures can be reduced and extremely packed structures limit cell migration and growth. After thorough cell viability and mechanical characterization, we used those formulations for the preparation of cell-laden hydrogels in

combination with C2C12 murine myoblasts and we evaluated the maturation of myotube structures by fluorescence microscopy. To this end, we used C2C12 laden composite hydrogels as a system to demonstrate the feasibility of the proposed technique in bioprinting constructs with preserved 3D structure over time. It was vital not only to match the morphology of the functional skeletal muscle fibers, but also the cellular arrangement. Control of the hydrogel properties, such as mechanical stiffness, swelling, degradation and porosity, was critical to obtain proper cellular function and tissue morphogenesis.

2. RESULTS AND DISCUSSION

2.1. Synthesis and characterization of methacrylated polymers

Our three composites bioinks incorporate four different photocrosslinkable materials (Fig. 1). GelMA emulates the ECM for various cells types [45] in combination with the non-biodegradable materials Alginate (Alg), carboxymethylcellulose (CMC) and PEGDA. GelMA is a photocrosslinkable hydrogel derived from natural gelatin. Gelatin was functionalized with methacrylate anhydride as described previously [45] and the methacrylation was characterized by a colorimetric assay. Hydrogels were finally fabricated using gelatin-metharyloyl with 40% degree of methacrylation (Table S1, supporting information). Alginate was methacrylated following the protocol described by Jeon et al. [28]. In addition, for the first time CMC was successfully functionalized using 2-aminoethylmethacrylate (AEMA) and EDC/NHS using carboxylic acids as anchorage points. The number of methacrylate groups was directly verified by ^{1}H-NMR and was in close agreement (Fig. 1 & 2, supporting information) with previous work [28, 34]. We assume that following reported protocol Alginate and CMC achieved a theoretical and real degree of

methacrylation about 45 % and 25% respectively [28, 34]. Finally, PEGDA, which has already two end acrylate groups, was obtained from a commercial supplier.

2.2. Assessment of optimal C2C12 survival after encapsulation in composite hydrogels

Cell viability after encapsulation in photocrosslinkable bioinks, are under the influence of several factors, such as material concentration[46], functionalization degree (amount of functional methacryltes/methacrylamides conjugated onto the polymer) [45], UV exposure time, type of photoinitiator and photoinitiator concentration [40]. For this reason, the limits of these factors controlling printing capabilities were assessed based on cell viability. To determine the most relevant factors acting on cell viability, C2C12 myoblasts were encapsulated using different biomaterial concentration, photoinitiator concentration, and UV exposure time. Two different photoinitiators were used, 2-hydroxy-4′-(2-hydroxyethoxy)-2-methylpropiophenone (I2959) and lithium phenyl(2,4,6-trimethylbenzoyl)phosphinate (LAP). To assess all these parameters a 2^4 ANOVA multifactorial analysis of cell viability assay was designed using 96 well-plates. Cell viability was determined 24 h after cell printing by an alamarBlue® commercial kit. % reduction of alamarBlue® reagent is related to cell metabolism, in this way high values of reduction mean high cell viability. Due to the bioprinter equipment used in this work the intensity of the UV light could not be adjusted, but the effects of this parameter were incorporated in exposure time. It is possible to increase or reduce the UV dosage by using longer or shorter exposure times, respectively.

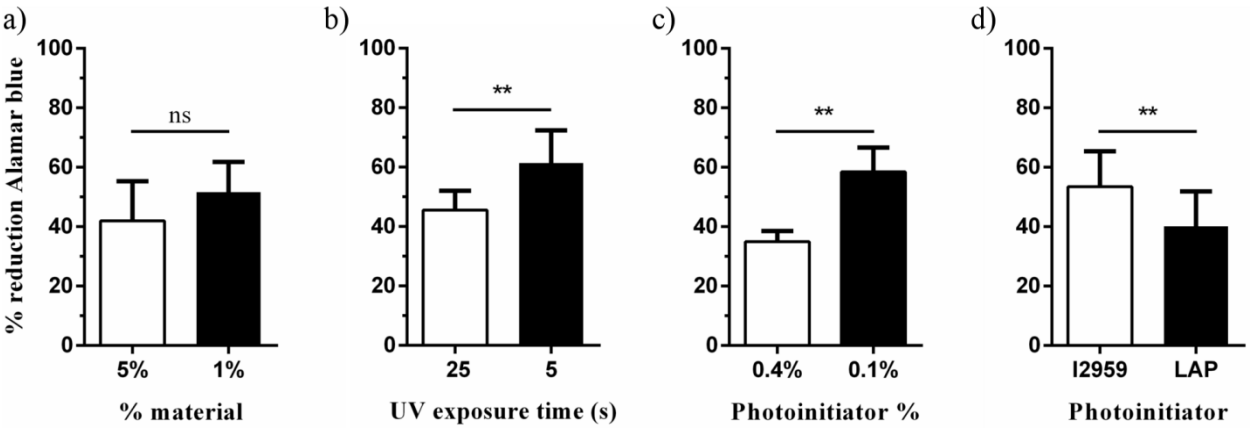

Figure 2. Effect of a) GelMA concentration, b) UV exposure time, c) photoinitiator concentration, and d) photoinitiator type on the C2C12 viability. C2C12 cells were encapsulated in GelMA hydrogels at 10^6 cell/mL and cultired for 24 h. Polymer solutions were prepared containing either I2959 or LAP photoinitiators at 0.1% or 0.4% w/v. Cell-laden prepolymers were photopolymerized under 25 s or 5 s of UV light. Cell viability was examined using the alamarBlue® test. Values are represented as % reduction (mean ± standard deviation, t-test ** $p<0.01$, n=12).

The full statistical dataset is shown in the supporting information. By extracting relevant information, it is possible to define the limits of the bioprinting system. In all samples, composites irradiated for less than 5 s were unable to crosslink. In addition, we found that cell viability was strongly affected by the exposure time, and 25 s of UV drastically reduced cell survival (Fig. 2b). Photoinitiator concentration has a strong effect on cell viability because the free radicals produced after UV exposure are cytotoxic. Figure 2c shows the mean cell survival of all samples fabricated with 0.1% and 0.4% of photoinitiator (LAP or I2959). This graph demonstrates that increasing the photoinitiator concentration (even I2959 or LAP) from 0.1% to 0.4% dramatically decreased cell survival. As was reported previously LAP has a higher extinction coefficient at 365 nm than I2959 [40], and more radicals are generated using the same concentration, this fact influence cell viability

and could explain why I2959 was less toxic than LAP (Fig 2d). In contrast, the quantity of material did not have a significant effect on the cell viability after printing. Below 1% of material, the structures obtained were not consistent enough to be useful and above 7% the high viscosity clogged the nozzle orifice.

Taking the alamarBlue® assay results and the preservation of the 3D structure of the hydrogels, we concluded that it is possible to work within the 5 s to 25 s range of UV exposure time. A 0.1% concentration of photoinitiator is the maximum level. It is possible to use both types of photoinitiators and finally work with 5% to 7% of material using methacrylated biomaterials in accord with previous findings [44].

2.3. Hydrogel swelling and degradation

To study the stability of the different hydrogels over time, different samples were prepared in concordance with the previous viability assay conditions. Crosslinking conditions were: 5% of GelMA material with 1% of non-biodegradable methacrylated biomaterial, 5 s of UV dosage and 0.1% photoinitiator concentration. As noted in the previous section, photoinitiator concentrations above 0.1% were discarded as unviable because of high cytotoxicity. Below 0.1% we observed high variability in the formation of the crosslinked scaffolds. Figures 3a and 3b show pictures of the fabricated cylinder-shaped hydrogels. Samples obtained with I2959 were too weak to maintain cilindrical shape, especially compared to hydrogels fabricated with LAP.

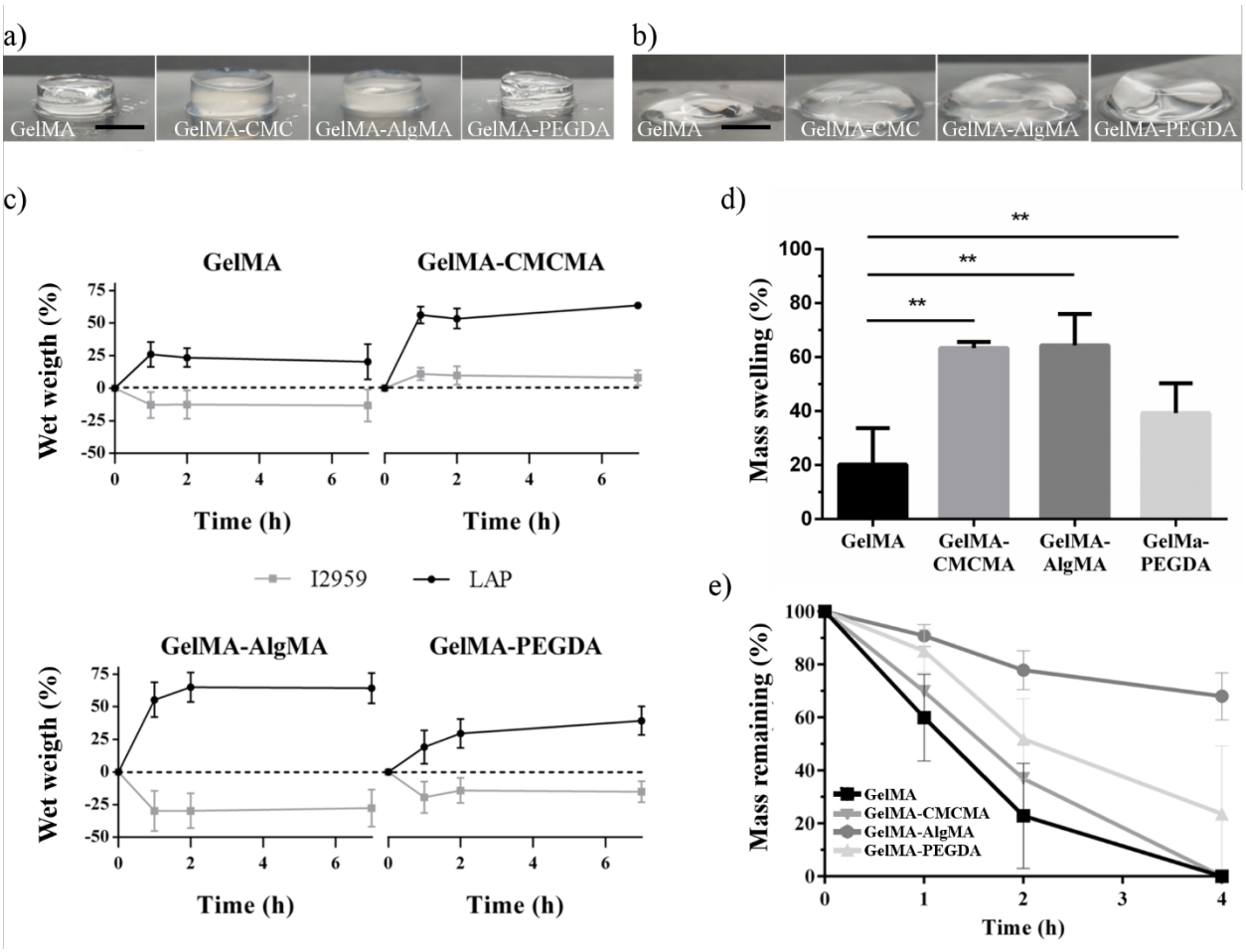

Figure 3. Effect of composites on the swelling and degradation of 5% w/v GelMA hydrogels. Disc shaped hydrogels fabricated using a) I2959 or b) LAP as a photoinitiator, under 5 s of UV light exposure. c) Swelling was studied as the change in wet weight d) and differences in mass were found in the case of CMCMA, PEGDA and AlgMA (mean ± standard deviation, ** $p<0.01$, n=6) at the equilibrium swelling. e) Percentage mass remaining profile showing the effect of the composite on the decrease in the wet weight of hydrogels (mean ± standard deviation, n=4) incubated in a 1.5 U/mL collagenase type II solution. GelMA (■), GelMA-CMCMA (▼), GelMA-AlgMA (●), GelMA-PEGDA (▲).

Wet weight increases as function of time in composite hydrogels made with both photoinitiators, I2959 and LAP (Fig. 3c). Samples were weighted after fabrication and after 1, 2 and 7 d. Photoinitiator molar extinction coefficient, ε, determines the generation of free radicals as a function of the wavelength. I2959 showed weak molar absorptivity ($\varepsilon = 4\ M^{-1}\ cm^{-1}$) at 365 nm [40, 47], and composite hydrogels had a wet weight increase close to 0% or even below, meaning a loss of mass. Thus, with 5 s of UV dosage composite hydrogels showed low crosslinking. The apparent low crosslinking resulted in a loss of material and in poorly manageable hydrogels. This behavior occurred due to the pore dilatation after water absorbance. Therefore, the negative values of wet weight increase are explained due to the loss of material, which was greater than the absorbed water content. This effect was not observed in the case of composite hydrogels made with LAP, which were easy to handle and showed wet weight increases > 25%. LAP has about 50-fold higher molar absorptivity ($\varepsilon = 218\ M^{-1}\ cm^{-1}$) at 365 nm than I2959 [40] which explains the results. Thus, the LAP hydrogels showed a normal swelling behavior, and after 7 d all reached the swelling equilibrium.

The dramatic effect on shape fidelity by using I2959 (Fig. 3b) could be also attributed to oxygen inhibition in the polymerization system, as has been recently published [48]. Lim et al. prove that shape fidelity is improved by increasing photoinitiator concentration or UV dosage. In our case, the LAP's higher molar absorptivity produces the same effect on the photopolymerization yield, and resulted in high fidelity, thickness and mechanical stability (Fig. 3a).

Combinations of GelMA with the hydrophilic methacrylated polymers, showed an increase in the final wet weight. Composite blends containing 1% of CMCMA (*p-value* = 0.0001), AlgMA *(p-value* = 0.013), or PEGDA (*p-value* = 0.04) showed significant differences and scaffolds with high water content and swelling were obtained (Fig. 3d). The differences in the water uptake could be

attributed to the highly hydrophilic structure of the polysaccharides. In the case of GelMA-AlgMA, the increase in swelling is in concordance with recent publications [37].

To study the effect of polymer composition on the degradation of composite hydrogels collagenase II (1.5 U/mL), which degrades gelatin fraction, was used. Samples were weighted after 1, 2 and 4 h. Hydrogels made in the presence of I2959 were completely degraded after 1 h due to their low crosslinked structure. For this reason, the results of the degradation of the materials obtained only with LAP are plotted (Fig. 3e). Compared with pristine GelMA the composite hydrogels showed more resistance to degradation. The addition of 1% PEGDA (*p-value* = 0.046) and AlgMA (*p-value* = 0.016) significantly decreased the degradation rate. In particular, more than a half of the mass swelling (68%) remained for GelMA-AlgMA hydrogels after 4 h of enzymatic degradation.

The results show the increased resistance to degradation of composite hydrogels by the addition of small percentage of non-mammalian animal derived polymers. Since Alginate, CMC and PEGDA are not degradable by mammalian cells [34, 49, 50] and provide stability to the composite hydrogels. It is important to note the better mechanical stability and long-lasting structures when fabricated with LAP.

2.4. Composite hydrogels with tunable mechanical properties

After swelling, hydrogels were punched to obtain 10 mm diameter cylinders and stress-strain curves were measured by Dynamic Mechanical Analysis (DMA). Young's modulus was calculated using a compressive modulus and was calculated as the slope of the linear part of the stress-strain curves. As the swelling results show (Fig. 3c), hydrogels made in the presence of I2959 under 5 s of UV exposure were extremely weak and it was not possible to perform the

mechanical measurements in some of them (Fig. 4a). In contrast, all the samples made in the presence of LAP under 5 s of UV exposure were easy to handle and the Young's modulus values were significantly higher (*p-value* < 0.005) than those of I2959. It was clear that I2959 needs high UV dosages to develop adequately crosslinked hydrogels and, for this reason, 25 s of UV exposure was used. With this UV dosage it was possible to fabricate stable hydrogels, but this exposure time reduced C2C12 viability (Fig. 2a).

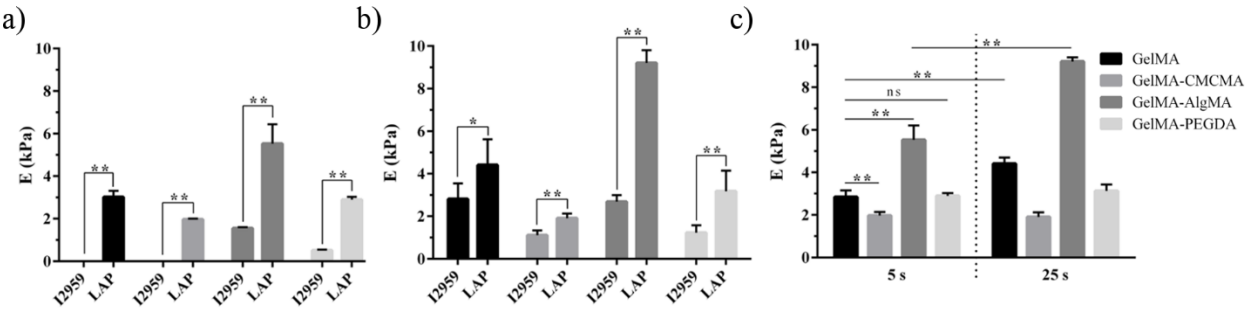

Figure 4. Characterization of the mechanical properties of the composite hydrogels. Young's Moduli of GelMA and the three composites photocrosslinked with I2959 and LAP during a) 5 s and b) 25 s. c) Comparative Young's Modulus of hydrogels photocrosslinked with LAP during 5 s and 25 s. Values are plotted as the mean ± standard deviation, ** p<0.01, n=3.

Increase in the polymer concentration, in particular GelMA, increases the stiffness properties of the hydrogel [47]. In our case, in the optimized conditions (using LAP and 5 s of UV exposure) Young's modulus was determined to be 3.02 ± 1.13 kPa for 5% GelMA. These values agree with reported by Nichol et al. (~ 2 kPa), Camci-Unal et al. (3.4 kPa), and Costantini et al. (2.45 – 5.81 kPa) where similar polymer percentage and degree of methacrylation are used [44, 45, 51]. Fig. 4b shows that the material stiffness had different behavior with the addition of 1% of PEGDA, CMCMA, and AlgMA. The addition of PEGDA (2.89 ± 0.46 kPa for GelMA-PEGDA) did not cause significant changes. However, addition of CMCMA caused a significant reduction in the

compressive moduli to 1.96 ± 0.16 kPa ($p < 0.05$). With AlgMA we observed the opposite effect, with the stiffness increasing significantly to 5.53 ± 2.01 kPa ($p < 0.05$).

In all cases, GelMA-AlgMA hydrogels showed the highest compressive modulus compared to the other composites. The mild gelation of alginate by the addition of divalent cations such as Ca^{2+} is widely used in biomedical applications. We could assume that the relevant differences of GelMA-AlgMA over the other composites are due to a secondary ionotropic gelation because of divalent ions contained in the polymer solution or in the PBS during the swelling.

Stiffness of composite hydrogels can be related to their resistance to collagenase degradation. GelMA-AlgMA hydrogels had the highest resistance and the lowest degradation, followed by GelMA-PEGDA and GelMA-CMCMA hydrogels. These results suggest that the crosslinking density of hydrogels depends on the composite material, UV dosage and type of photoinitiator. Furthermore, as previously indicated, the mechanical properties of hydrogels strongly impact muscle function and phenotype [39, 42-44, 52]. Therefore, it is of great interest to make hydrogels mimicking the biological scaffolds with tunable mechanical properties. It is possible to increase the mechanical properties of hydrogels as to increase the hydrogel concentration, the UV dosage or the photoinitiator. However, these methods may reduce cell viability, as we have demonstrated, and the porosity and interconnectivity of hydrogels and therefore has adverse effects on performance of hydrogels [53]. For example, it has been demonstrated that increasing the mechanical properties of GelMA hydrogels by increasing the concentration and/or molecular weight of methacrylate limited cell viability and growth, morphogenesis, and cell migration [54]. In this regard, non-degradable materials hold a great promise as a supplementary material for hydrogels to tune their mechanical properties. Due to their different chemical structures, small amount of these non-degradable materials is sufficient to considerably change the mechanical

properties of composite hydrogels with minor effect on cells encapsulated. Finally, all composite hydrogels were shown viscoelastic behavior in the range of the stiffness to promote myotube differentiation in 3D (1-3 kPa) [44] and in 2D structures (8-11 kPa) [55, 56]; therefore, all of them could be ideal scaffolds for soft tissues, such as skeletal muscle.

2.5. Pore size and pore distribution

The pore size of composite hydrogels was analyzed using Scanning Electron Microscopy (SEM). The images revealed that the fibrillar structure of the gelatin was not affected by the addition of the other polymers. These images were therefore used to determine the pore size distribution. Among the different composite hydrogels, no significant differences were found in the range of the small pores (< 20 nm), which could limit the passage of nutrients and proteins [57]. However, GelMA-PEGDA hydrogels showed significant reduction in the number of pores with diameters > 200 nm ($5 \cdot 10^5$ nm^2). The GelMA-PEGDA hydrogel presented a homogenous structure in terms of pores size and pores distribution. The structure is more packed as we can see in figure 5d, and the total amount of pores > 200 nm was below 0.05% of the total pores (Fig. 5f). This porosity range between 200 and 600 nm is where cells can best spread and extrude their filopodia [58-60]. Therefore, very low levels or the nonexistence of pores above this size could reduce cell viability because the limited cell spreading. Furthermore, the absence of these pores can negatively affect skeletal muscle differentiation, where myoblast spreading, and cell-cell contact play key role in myotubes formation [13].

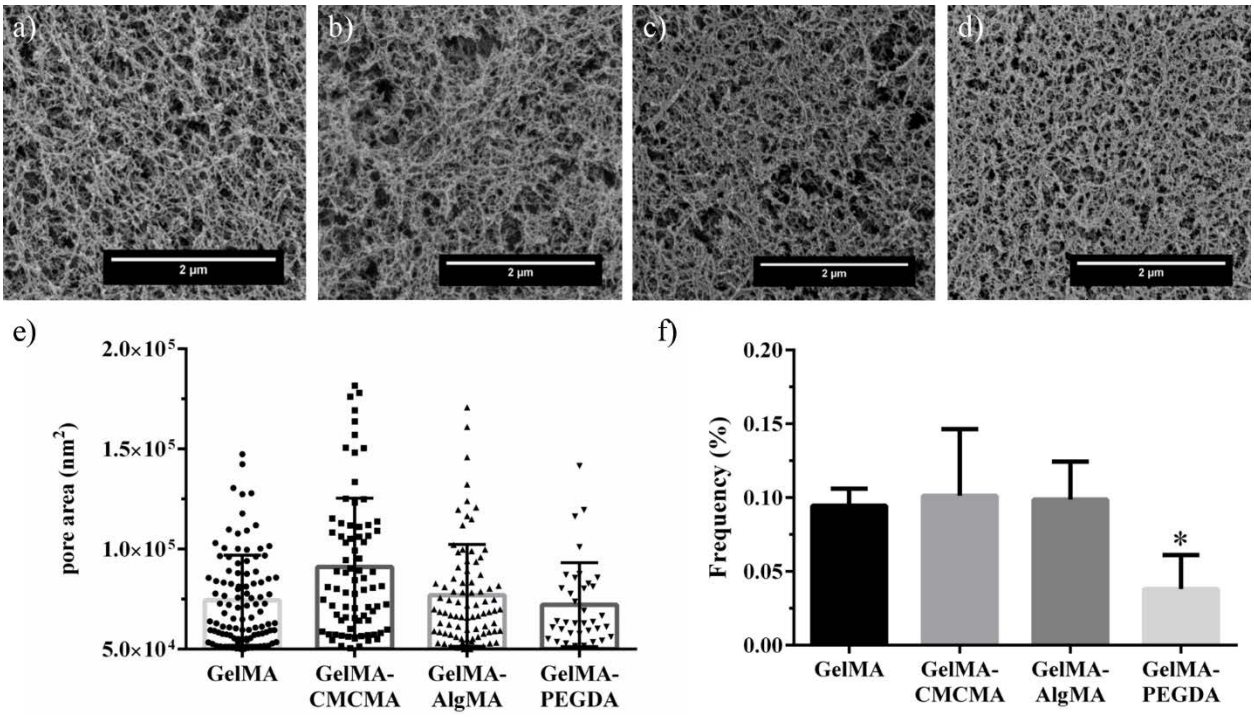

Figure 5. Scanning Electron Microscopy (SEM) images of a) GelMA, b) GelMA-CMCMA, c) GelMA-Alg, and d) GelMA-PEGDA. The aqueous part of composite hydrogels was removed after critical point drying and fibrillar structure of GelMA was left behind. e) Pore size distribution above 200 nm in diameter and f) their fraction of the total pore population, expressed as percentages (mean ± standard deviation, * $p<0.05$).

We kept the concentrations of CMCMA, AlgMA and PEGDA constant but increasing this concentration will affect the physico-mechanical properties of the composite hydrogels. Swelling behaviour should show an increase [34], and then a decay because of increasing the polymer concentration. Moreover, composite hydrogels would be more resistant to biodegradation [51]. Compressive moduli and pore size will also be affected by increasing the non-degradable compounds concentration. As has been published, an increase on AlgMA content makes the hydrogels stiffer and reduces the pore size [37]. In the case of CMCMA, it seems to induce, first, a

softening of the hydrogels, but the further increase of polymer concentration should lead to a stiffening effect.

2.6. Long term C2C12 viability and proliferation within composite hydrogels

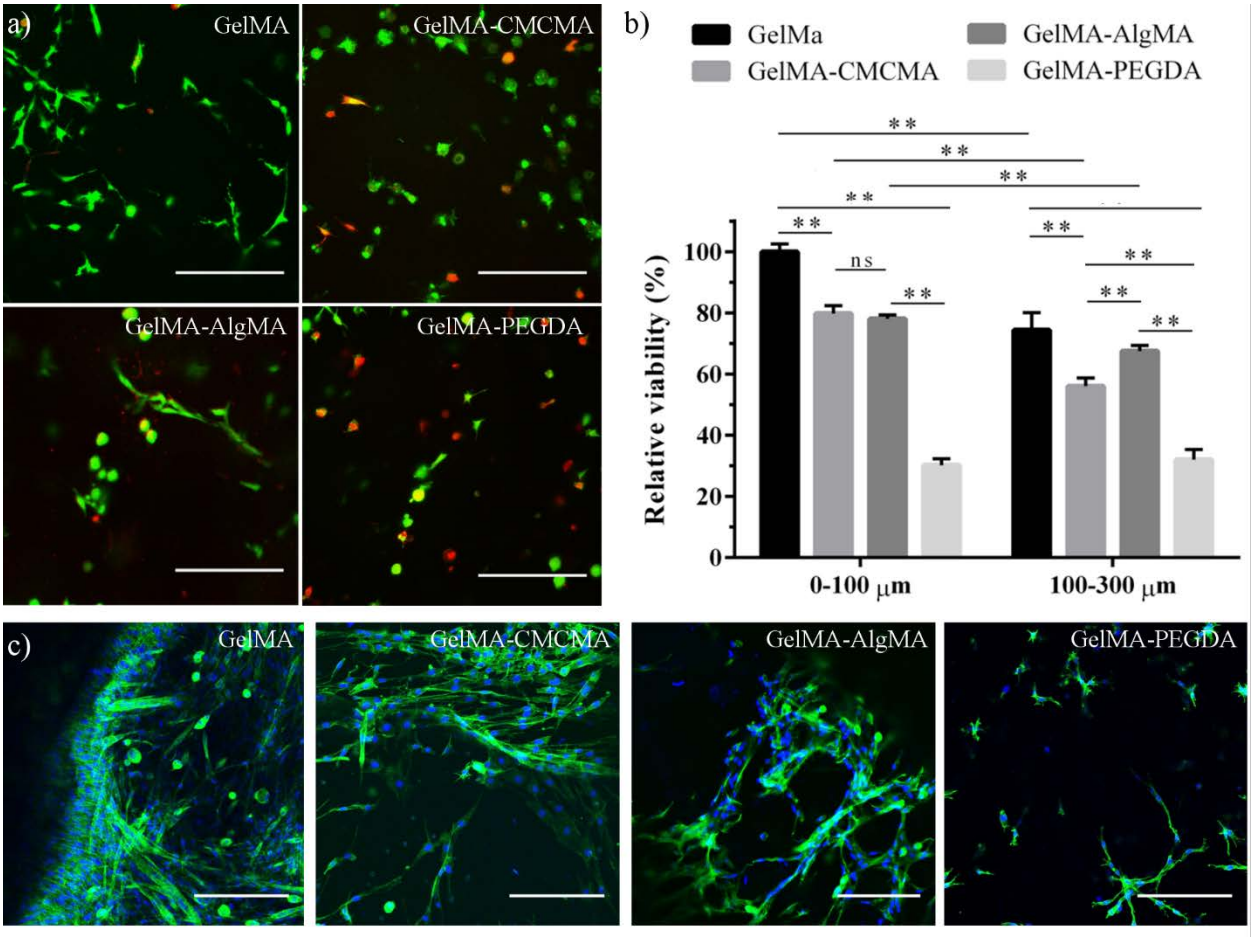

Figure 6. C2C12 viability and proliferation in the composite hydrogels at 7 d. a) Representative images of the Live/Dead staining (dead in red and live in green) in the range of the first 100 µm depth. b) Cell viability in composite hydrogels represented as the living cells over the total cell number (mean ± standard deviation, ** $p<0.01$) relative to GelMA hydrogels. c) Confocal microscopy pictures of C2C12 cells inside composite hydrogels. F-actin in green and nuclei in blue. Scale bar = 200 µm.

In this study, we compared the long-term viability of C2C12 encapsulated in the composites hydrogels using GelMA as the positive benchmark. To study the long-term viability and proliferation of C2C12 cells, 5% (w/v) GelMA was dissolved in PBS buffer, with LAP 0.1% and 1% of either PEGDA, CMCMA, AlgMA was added to the polymer solutions corresponding to composites. Cells were trypsinized and the cell suspension was prepared in growth medium. The material and the cell suspension were mixed in 1:1 proportion and a drop of the resulting solution was immediately placed in a previously mounted PDMS mold. The samples were irradiated for 5 s under UV light and allowed to swell in growth medium. The final structures, after demolding, had a 6 mm diameter size and 750 µm height.

The percentage of living cells in the hydrogels was determined using the Live/Dead staining kit at 1 and 7 d. The viability obtained in the GelMA hydrogels was about 80% at 1 d, in agreement with previous studies [61], and about 60% for GelMA-CMCMA and GelMA-AlgMA hydrogels These composite hydrogels showed a similar slight decrease in the cell viability at day 7 (Fig. 6a and 6b). The chemical structures of CMC and Alginate do not promote cell attachment to the surface, so they usually show lower survival values [35, 41]. However, in the composite materials, the viability was still high, and the values were similar to GelMA. Moreover, the percentage of living cells increased at 7 d (Fig. 6a and 6b). In contrast, the number of living cells in GelMA-PEGDA composites decreased dramatically after 1 d and low levels of living cells remained up to 7 d. These results could be explained by the reduction of the number of pores > 200 nm, in the GelMA-PEGDA hydrogels. Thus, cells remained immobilized after 1 d and their limited spread affected cell survival and produced low viability values.

We also observed that the number of dead cells increased in the deepest regions of the 3D structures. GelMA, GelMA-CMCMA and GelMA-AlgMA had significant differences between the

number of live cells counted within first 100 µm from the surface and the ones below 100 µm (until 300 µm) (Fig. 6b). The porosity of the materials determines the diffusion of nutrients inside the hydrogel. If nutrient uptake is faster than nutrient renewal through diffusion of the medium inside the hydrogel, a lack of nutrients results that increases with the material depth.

The ability of cells to attach, spread, and grow on hydrogels is important for tissue development [62, 63]. To check the proliferation, cell morphology, and distribution in the composites, immunofluorescence staining of F-actin and nuclei was performed (phalloidin and DAPI) at 7 d. Figure 6c shows cell spreading inside the hydrogels. C2C12 cells in GelMA-PEGDA were less spread than the other composites, with slight cytoskeleton protusions, which indicated that PEGDA impairs cell spreading. In contrast, in GelMA, GelMA-CMC, and GelMA-AlgMA C2C12 cells elongated inside the hydrogels, abundant F-actin filaments, and interconnected between them. These results indicated that GelMA-PEGDA is the less suitable candidate to promote C2C12 cell growth and spreading, compared to the pristine GelMA and those that contain CMCMA and AlgMA.

Stiffer materials in 2D are known to promote cell proliferation and attachment [25, 63]. Another important factor is the presence of cell adhesion sequences such as arginylglycylaspartic acid (RGD) [25]. In 2D, stiffness is a key factor but in 3D the porosity also influences cell proliferation and spreading as seen in our results. GelMA-PEGDA and pristine GelMA had no significant Young's moduli differences (Fig. 4c) but cell behavior in the hydrogel is totally opposite.

Even though GelMA-CMCMA composites are softer than GelMA-PEGDA composites, proliferation and cell adhesion are improved in GelMA-CMCMA. Altogether, the results are consistent with previous studies demonstrating that in 3D, muscular cells can spread, proliferate and present better myogenesis in less packed structures [44]. Our data suggests that stiffness is not

the main factor affecting cell behavior in 3D but rather the key factor is to obtain less packed structures with a good distribution of big pores. Here, we have obtained a library of composite materials with a good balance between the mechanical and mass transport function. As a result, we can choose between scaffolds with similar Young´s moduli values but with different pore sizes frequency.

2.7. Composite hydrogels as a bioink for muscle tissue bioprinting

Hydrogel patterning is widely used to align cells and. Extrusion bioprinting was used to build 3D scaffolds of C2C12 embedded in composite hydrogels. A C2C12 cell suspension was first mixed with the prepolymer solutions. The effect on cell alignment inside GelMA filaments below 200 μm in width has been already reported [54, 64], for this reason the mixture was introduced into a printing syringe and a nozzle of 200 μm inner diameter was used. Several filaments were drawn inside a circle. To achieve a relevant height (about 200 μm) two layers were printed (Fig. 7). In extrusion bioprinting, nozzle inner diameter, printing pressure, and rate can determine the width and the thickness of the printed bioink. After printing, filament width differed respect to the nozzle inner diameter, above 200 μm in diameter. Printing fidelity was evaluated as the percentage change in width. With this method, bioprinted structures were successfully made using GelMA, GelMA-CMCMA, GelMA-AlgMA and GelMA-PEGDA. Filaments of 200 μm in height and 200 μm in width were achieved and these could avoid the problem of low nutrient diffusion in thick hydrogels (Fig. 7a-c).

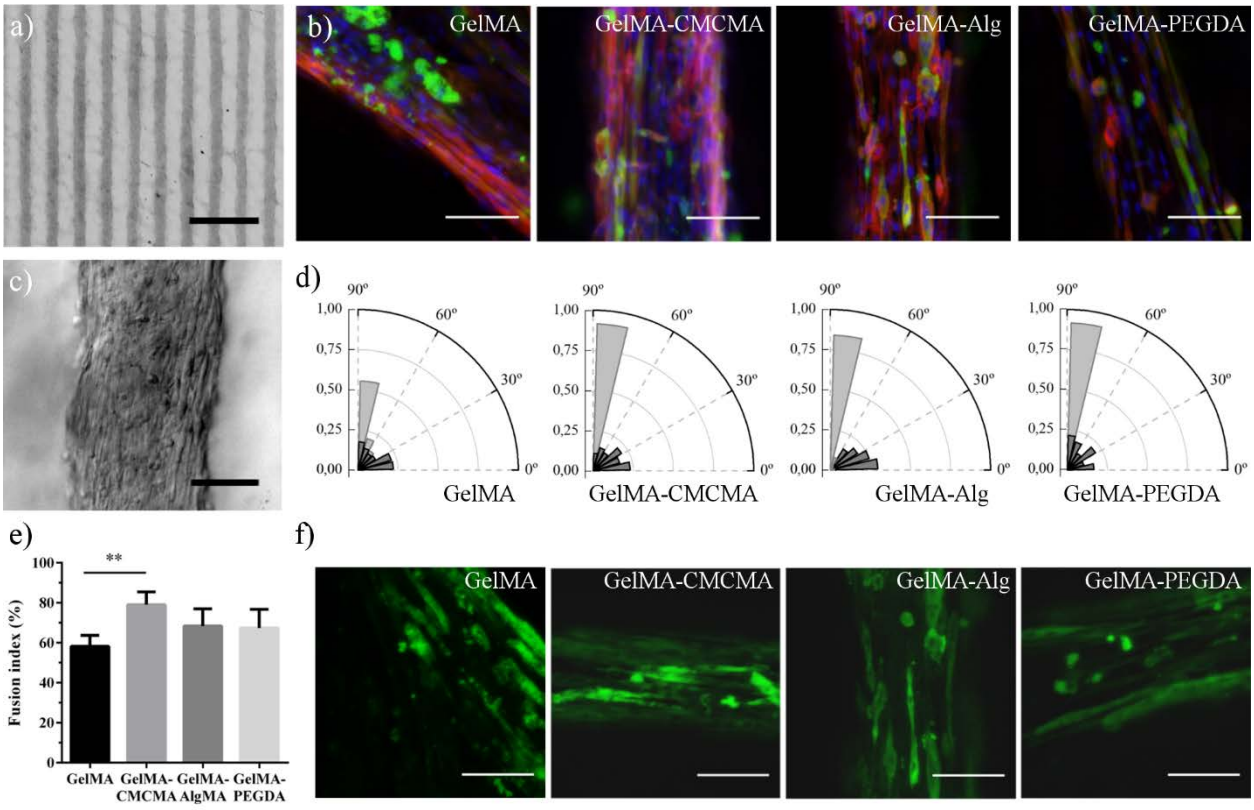

Figure 7. C2C12 myotube formation in bioprinted composite hydrogels. a) Bright field image of the bioprinted tubes after fabrication. Scale bar = 2 mm. 3D structure was successfully printed and remained stable after swelling. b) Confocal microscopy pictures of C2C12 cells encapsulated in the composite hydrogel structures after 11 d of culture. F-actin in red, MHC in green, and nuclei in blue. Scale bar = 200 µm. c) Bright field image of elongated cells encapsulated in composite hydrogel. Scale bar = 200 µm. d) Normalized histograms (bin = 10º) depicting the distribution of the angles between cell cytoskeleton fibers (light gray) inside non-patterned hydrogels (dark gray) and in 3D printed hydrogels. C2C12 inside the bioprinted hydrogels show high degree of alignment (>75%) following the pattern direction, while inside cylinder-shaped hydrogels are randomly distributed. e) Fusion index percentage (mean ± standard deviation, ** $p<0.01$) of the C2C12 myotubes encapsulated in the bioprinted composite hydrogels. f) Confocal

microscopy images showing the expression of MHC (green) in the C2C12 myotubes inside 3D bioprinted composite hydrogels. Scale bar = 200 μm.

Cells were cultured in growth medium until high confluence was reached (5 d) and then, growth medium was switched to differentiation medium. At 11 d, GelMA scaffolds were nearly flat, and the structure was lost, due to the cell activity (degradation) [ref] while the composite hydrogels preserved their 3D structure. To observe the morphology of the cells and distribution in the hydrogels, cells were stained with phalloidin and DAPI, and also stained with anti-Myosin Heavy Chain (MHC), a protein overexpressed only in differentiated striated muscle. In all cases, C2C12 were able to proliferate embedded in the composites and displayed myotube formation (Fig. 7b). The effect of the 3D structures on guiding cell alignment was confirmed by the analysis of myotube orientation (Fig. 7d). Patterned composite hydrogels exhibited unidirectional orientation of myotubes instead of a random, unorganized mesh as seen in the images obtained from the unpatterned hydrogels (Fig. 6c). Wider filaments were also fabricated and was observed that cell alignment reduced (X) considerably in the filament direction (Fig. S7 Supporting information). In agreement, it has been reported that cells confined in GelMA hydrogels, with a geometry constrain below 200 um widths induce high cell alignment [54]. Recently, the effect of 3D scaffolds with anisotropic morphology on cell alignment has also been demonstrated, where more than 60% alignment efficacy along 14 day of cell culture is proved [64]. In addition, shear stress generated in the nozzle helps the polymer chains to redirect parallel to the longitudinal axis of the bioink stream, thus also may promote the alignment of cell adhesion motifs. On the

Confocal images showed that MHC was present in all the constructs, indicating that it was possible to obtain differentiated myotubes. To evaluate the quality of differentiation in the patterned scaffolds, the fusion index was determined as the percentage of nuclei associated with

myotubes compared to the total number of nuclei in each sample [65, 66]. As expected, C2C12 fused into myotubes in GelMA hydrogel after 11 d of culture. GelMA-CMCMA and GelMA-AlgMA also promoted myogenesis (Fig. 7b and 7f). Furthermore, the fusion index of those composites was slightly higher than GelMA (Fig. 7e). As previously mentioned, GelMA 3D structures tended to degrade after several days due to cell metabolism making it difficult to find significant 3D areas comparable with the scaffolds made of composite materials. The fusion index corresponding to GelMA-PEGDA hydrogels was similar to the other composites immunofluorescence images indicating that the number of myotubes was significantly lower (Fig. 7e).

After all, has been proved the applicability of these composite hydrogels in skeletal muscle tissue engineering and for the first time, GelMA-CMCMA composite hydrogels have been successfully used to fabricate skeletal muscle constructs. Considering the adjustability of the physical properties, these composite hydrogels can be used in other tissue engineering applications: heart, cartilage, or bone as other authors have been demonstrated by using GelMa and AlgMA [32, 37].

3. CONCLUSION

3D bioprinter technologies have emerged as great system to fabricate complexes tissues and bioinks play a key role in such technologies. In this work, the influence of mechanical stiffness and geometrical confinement on the 3D culture of myoblast-laden GelMA photo-crosslinkable composite hydrogels was evaluated in terms of *in vitro* myogenesis. We compared new composites hydrogels (GelMA-CMCMA and GelMA-AlgMA) to print stable and not biodegradable skeletal muscle structures, and at the same time with tunable properties to allow high cell viability and myogenesis. Compared with non-degradable previously described composites hydrogels, such as GelMA-PEGDA, we obtained higher cell proliferation and viability. We demonstrated that frequency and presence of pores with diameters > 200 nm ($5 \cdot 10^5$ nm^2) are crucial factors in the

design of 3D scaffolds and in cell 3D encapsulation, even in hydrogels with different stiffness. The use of GelMA-CMCMA and GelMA-AlgMA composites with bioprinting methods allowed us to efficiently obtain 3D durable structures of differentiated and aligned muscle fibers. In contrast to GelMA, they are long-lasting materials and good candidates as hydrogels for *in vitro* applications and bio-actuators.

4. MATERIAL AND METHODS

4.1. Synthesis of polymer precursors

Gelatin (Sigma- Aldrich, USA) was modified to a 40% degree of methacrylation as previously described [14]. Briefly, gelatin was dissolved in PBS 10 mM at a concentration of 10% (w/v), and methacrylic anhydride (Sigma-Aldrich, USA) was carefully added to the solution drop by drop. One hour later, the reaction was stopped by adding an excess of PBS 10 mM and dialysed against Milli Q water with 6-8 kDa MWCO membranes (Spectra/por, Spectrumlabs, USA). Water was changed every 4 h during a 4 d period. Gelatin-methacryloyl (GelMA) was lyophilized and stored at -20 ºC. Sodium carboxymethylcellulose (CMC) and sodium alginate (Alg) (Sigma-Aldrich) were methacrylated at a maximum degree of methacrylation as previously described [39]. The methacrylation reaction was performed by mixing a solution of 1% (w/v) of the polymer in 50 mM MES buffer at pH 6.5 with 20 mM EDC, 10 mM N-hydroxysuccinimide and 10 mM 2-aminoethylmethacrylate (Sigma-Aldrich). The reaction was stopped after 24 h with the addition of acetone (Panreac, Spain) and filtered using a vacuum flask. The precipitate was dissolved in PBS 10 mM and dyalized against Milli Q water with 3.5 kDa MWCO membranes (Thermofisher, USA). Finally, the solutions of methacrylated polymers (CMCMA and AlgMA) were lyophilized and stored at -20 ºC.

4.2. Nuclear magnetic resonance

For ^{1}H-NMR, gelatin, GelMA, CMC, CMCMA, alginate and AlgMA were dissolved in D_2O and analyzed on a Varian Inova 500 (Varian, USA). All samples were measured with a relaxation delay of 1 second for 64 scans.

4.3. Preparation of prepolymer solutions

The polymer precursors (GelMA, CMCMA, AlgMA, and PEGDA) were mixed at different concentrations and diluted in PBS 10 mM containing the photoinitiator. Final concentrations of photoinitiator, either 2-Hydroxy-4′-(2-hydroxyethoxy)-2-methylpropiophenone (I2959) (Sigma-Aldrich) or lithium Phenyl (2,4,6-trimethylbenzoyl)phosphinate (LAP) (TCI EUROPE N.V., Belgium) were fixed at 0.4% or 0.1% (w/v). Polymer solutions were placed at 65 ºC for 1 h to obtain homogeneous solutions. Polymer solutions were prepared to obtain final concentrations of 5% or 1% (w/v) GelMA and 1% (w/v) CMCMA, AlgMA, or PEGDA. All hydrogels were fabricated using a 3D bioprinter (3DDiscovery™ BioSafety, regenHU, Switzerland; 365 nm, 3 W/cm^2) with the UV light source..

4.4. Multifactorial analysis to assess cell viability under 3D bioprinting conditions

The alamarBlue® assay (Thermofisher) was performed by following manufacturers protocols. A multifactorial screening was assessed to test the synergic effect of GelMA concentration, photoinitiator concentration of both I2959 and LAP, and UV exposure time, on the cell viability. Prepolymers were prepared at 1% or 5% w/v of GelMA. Photoinitiators were used at 0.1% and 0.4% w/v. Cell-laden hydrogels (20 uL amounts) (10^6 C2C12 cells/mL) were poured into cells of a 96 well-plate. After UV exposure, samples were rinsed with growth medium to remove unreacted reagents and cultured for 24 h. Then, samples were incubated with alamarBlue® solution at 10%

v/v in growth media for 3 h at 37ºC. Finally, the absorbance was read at 570 nm (λ_1) and 600 nm (λ_2). The percentage of reduction (cell viability) was determined by the following equation:

$$\%\ Reduction = \frac{(\varepsilon_{OX})\lambda_2 \cdot A\lambda_1 - (\varepsilon_{OX})\lambda_1 \cdot A\lambda_2}{(\varepsilon_{RED})\lambda_2 \cdot A'\lambda_1 - (\varepsilon_{RED})\lambda_1 \cdot A'\lambda_2} \cdot 100$$

Here, ε_{OX} and ε_{RED} represent the molar extinction coefficient of alamarBlue® oxidized form. A and A', represent the absorbance of the samples and the negative control, respectively. Statistical comparison was performed using a 2^4 ANOVA multifactorial analysis by StatGraphics Centurion software (Supporting information).

4.5. Swelling analysis of composite hydrogels

The prepolymer solutions were prepared as described above. Samples for swelling analysis were prepared by placing 300 µL of the prepolymer solution in a 48 well plate. After exposing the prepolymer solution to UV light hydrogels were rinsed with PBS and their initial weight was measured. Then, the wet weight was determined after 1, 3, and 7 d in PBS, after a wipe with tissue paper to remove the excess water. The wet weight increase ratio (ΔW) of the hydrogels was determined by the following equation:

$$\Delta W = \frac{W_s - W_i}{W_i} \cdot 100$$

Here, W_i and W_s represent the weight of composite hydrogels after fabrication and the weight after swelling in PBS, respectively. To calculate the mass increase, each water content value was normalized with the initial weight of the sample

4.6. Degradation of composite hydrogels

Hydrogels were fabricated as described above for the swelling analysis. Hydrogels were removed from the 48 well-plate and left swelling for 3 d in a 6 well-plate. A total of 3 mL of 1.5 U/mL of collagenase type II (Thermofisher) in PBS was added on the hydrogels and they were incubated at 37ºC, under 100 rpm shaking conditions. Then, hydrogels were weighted after 1, 2 and 4 h. The percent hydrogel remaining (%W_r) was determined by the following equation:

$$\%W_r = \frac{W_t}{W_i} \cdot 100$$

Here, W_t represents the weight of hydrogel composites after collagenase incubation.

4.7. Analysis of the Mechanical Properties of composite hydrogels

Uniaxial compression tests of hydrogels were performed using a Zwick Z0.5 TN instrument (Zwick-Roell, Germany) with a 5 N load cell. Hydrogels were fabricated following the same procedure as for the swelling analysis. After reaching equilibrium swelling, cylindrical hydrogels were cut using a 10 mm diameter biopsy punch. Real hydrogel diameters and heights were measured prior to the experiment. Samples were tested at room temperature up to 30% final strain (deformation), using the following parameters: 0.1 mN preload force and 20%/min strain rate. Stress-strain graphs were obtained from load-deformation measurements. Values for the compressive modulus were calculated from the slope of the linear region corresponding to 10-20% strain. For each hydrogel formulation, three samples were prepared, and measurements were performed in triplicate.

4.8. Pore size quantification

Cylinder-shaped hydrogels, 10 mm in diameter, were fabricated as described above for pore size quantification. Then, they were left swelling in Milli-Q water for 3 d to reach the same hydrogel architecture as cell encapsulation experiments and be comparable with them After that, dehydration was carried out by sequential immersion in graded ethanol solutions in Milli-Q water: 30%, 50%, 70%, 80%, 90%, and 96% v/v for 5-15 min each and twice for 100% ethanol. Then, samples were placed in the chamber of a critical point dryer (K850, Quorum technologies, UK), sealed and cooled. Ethanol was replaced completely by liquid CO_2, and by slowly heating. CO_2 achieved gas phase equilibrium at 35°C and 85.06 atm and was slowly drained. This technique allowed dehydration of the hydrogels while avoiding their collapse. After critical point drying, hydrogels were imaged by ultrahigh resolution scanning electron microscopy (Nova™ NanoSEM 230, FEI Company, The Netherlands) operating in low vacuum mode (0.5 mbar of water vapor pressure). SEM images were used to quantify the pore size distribution by the use of ImageJ free software (http://rsb.info.nih.gov/ij, National Institutes of Health, USA).

4.9. 3D culture of C2C12 myoblasts embedded in the composite hydrogels

C2C12 myoblasts from *Mus musculus* were purchased from ATCC and expanded in growth medium based in Dulbecco Modified Eagle Medium (DMEM high glucose, L-Glutamine, Gibco, Thermofisher) supplemented with 10% fetal bovine serum (FBS) (Thermofisher) and 1% penicillin/streptomycin (Thermofisher) at 37 ºC and 5% CO_2 atmosphere. To promote myotube formation, differentiation medium was used, based in DMEM high glucose and L-Glutamine, supplemented with 2% Horse Serum (HS) (Thermofisher) 1% Penicillin/Streptomycin, and 2.5% HEPES (Thermofisher).

To fabricate cell-laden hydrogels, one volume of prepolymer solutions of the different composite hydrogels was mixed with one volume of a suspension of C2C12 cells to a final density of 1 x 10^7 cells/mL. Blends of prepolymer and cells were then placed in a cylindrical mold of 6 mm inner diameter and 750 µm height. Cell-laden solutions were photocrosslinked by 5 s or 25 s exposure to UV light at 3 W/cm^2. This was followed by immersion of the cell-laden hydrogels in growth media to remove the unreacted reagents.

4.10. C2C12 survival in the composite hydrogels

C2C12 cells were encapsulated in each hydrogel as described previously. The viability was studied after 1 and 7 d using the Live/Dead Assay Kit and Hoechst (Thermofisher). Fluorescence images were captured using confocal microscopy (TCS SPE, Leica, Germany) and processed by MATLAB software (Supporting information). Survival percentage was calculated as the fraction of living cells in respect to the total cell number. Additionally, cell morphology within the hydrogels was studied through the immunostaining of nuclei and filamentous actin (F-actin). For this purpose, hydrogels were fixed in 10% formalin solution (Sigma-Aldrich) at 7 d after fabrication. Then, hydrogels were washed with PBS and cells were permeabilized with Block-Perm solution: 0.2% v/v Triton X-100 (Sigma-Aldrich) and 1% w/v BSA (Sigma-Aldrich) in PBS for 1 h. Afterwards, hydrogels were washed in PBS and incubated in 100 nM Rhodamine Phalloidin 480 (Cytoeskeleton, USA) solution overnight. After washing with PBS, nuclei were counterstained with DAPI (300 nM, Thermofisher) for 15 min. Hydrogels were mounted and stored at 4 ºC before observation by confocal microscopy.

4.11. C2C12-laden composite hydrogels bioprinting and C2C12 differentiation into myotubes

Prepolymer solutions and C2C12 cell suspension were mixed as previously described to obtain a 5% w/v GelMA solution with or without 1% of either PEGDA, CMCMA, or AlgMA in PBS containing 0.1 % w/v LAP. Solutions were introduced in a 3-cc printing syringe (Nordson Corporation, USA) and placed in the direct dispensing head of the bioprinter (3DDiscovery™ BioSafety). All of the printing processes were performed in a cooling chamber at 10 ºC. The printing rate was 7 mm/s and printing pressure varied between 1 to 2 bars depending on the loaded prepolymer solution. To promote myotube formation and alignment, cell-laden hydrogels architecture was designed as an array of 20 filaments in a 16 mm diameter circle (BioCAD v1.0 software, regenHU Ltd., Switzerland), and converted to computer-aided design (CAD) files (Fig. S6, Supporting information). CAD files were opened in the 3D DISCOVERY HMI software interface (regenHU Ltd., Switzerland). Constructs were made by the extrusion of two layers, by using a nozzle of 200 µm inner diameter, and then were photocrosslinked by a 5 sec exposure to UV light (365 nm) into a 6 well-plate. After that, hydrogels where immersed in growth medium and changed three times to remove unreacted reagents. After 5 d, growth medium was switched to differentiation medium. Samples were fixed at 11 d and F-actin and nuclei were stained as described previously (Section 4.10). In addition, a staining of myosin heavy chain was performed by incubating the samples in in a 5 µg/mL MF20 Alexa Fluor 488 (eBioscience, Thermofisher) solution overnight

4.12. Myotube alignment and Fusion index analysis

Z-stack images obtained by confocal microscopy were processed using ImageJ software. MHC staining was used for analysis of the fusion index and myotube alignment. Myotube alignment was assessed by measuring the angle formed between the myotubes and the longitudinal axis of the printed pattern. The fusion index was calculated by dividing the number of nuclei within myotubes

by the total number of counted nuclei and this was expressed as a percentage. Three samples for each condition were used and more than 100 myotubes were analyzed for each sample.

4.13. Statistical analysis

All data collected were presented as the mean ± standard deviation (SD) using GraphPad Prism software (GraphPad, USA). ANOVA and t-tests were performed in StatGraphics Centurion software (StatGraphics, Spain) to compare treatments. A *p-value* of 0.05 or less was considered statistically significant.

ASSOCIATED CONTENT

Supporting information

Supporting Information is available from the Wiley Online Library or from the author.

AUTHOR INFORMATION

Corresponding author

* Corresponding authors: Dr. Javier Ramon-Azcon, Biosensors for Bioengineering group, Institute for Bioengineering of Catalonia (IBEC), The Barcelona Institute of Science and Technology (BIST), c/ Baldiri Reixac 15–21, 08028 Barcelona, Spain

E-mail: jramon@ibecbarcelona.eu

Prof. J. Samitier, Nanobioengineering group, Institute for Bioengineering of Catalonia (IBEC), The Barcelona Institute of Science and Technology (BIST), c/ Baldiri Reixac 15–21, 08028 Barcelona, Spain

E-mail: jsamitier@ibecbarcelona.eu

Department of Electronic and Biomedical Engineering, University of Barcelona, c/ Martí i Franqués 1, 08028 Barcelona, Spain

Centro de Investigación Biomédica en Red en Bioingeniería, Biomateriales y Nanomedicina (CIBER-BBN)

Author contributions

[a] These authors contributed equally to this work

Notes

ACKNOWLEDGMENTS

Funding for this project was provided by the Ramon y Cajal (RYC-2014-15022) fellowship and Severo Ochoa Program for Centers of Excellence (R&D 2016- 2019) funded by the Ministerio de Economía, Industria y Competitividad; an ERC grant (ERC starting grant project – 714317 – DAMOC); the CERCA Programme/Generalitat de Catalunya (2014-SGR-1442 and 2014-SGR-1460); and the Fundación Bancaria "la Caixa"- Obra Social "la Caixa" (projecte IBEC-La Caixa Healthy Ageing); MINDS project funded by MINECO (TEC2015-70104P) and Biobot TEC2015-72718-EXP.

REFERENCES

[1] S. Ahadian, R. B. Sadeghian, S. Salehi, S. Ostrovidov, H. Bae, M. Ramalingam, A. Khademhosseini, *Bioconjugate Chemistry* 2015, *26*, 1984.
[2] S. Ostrovidov, V. Hosseini, S. Ahadian, T. Fujie, S. P. Parthiban, M. Ramalingam, H. Bae, H. Kaji, A. Khademhosseini, *Tissue Engineering Part B-Reviews* 2014, *20*, 403.
[3] J. M. Grasman, M. J. Zayas, R. L. Page, G. D. Pins, *Acta Biomaterialia* 2015, *25*, 2.
[4] P. Banerjee, A. K. Bhunia, *Trends in Biotechnology* 2009, *27*, 179.
[5] T. G. Fernandes, M. M. Diogo, D. S. Clark, J. S. Dordick, J. M. S. Cabral, *Trends in Biotechnology* 2009, *27*, 342.
[6] S. B. Kim, H. Bae, J. M. Cha, S. J. Moon, M. R. Dokmeci, D. M. Cropek, A. Khademhosseini, *Lab on a Chip* 2011, *11*, 1801.
[7] N. Misawa, H. Mitsuno, R. Kanzaki, S. Takeuchi, *Proceedings of the National Academy of Sciences* 2010, *107*, 15340.
[8] N. S. Bhise, J. Ribas, V. Manoharan, Y. S. Zhang, A. Polini, S. Massa, M. R. Dokmeci, A. Khademhosseini, *Journal of Controlled Release* 2014, *190*, 82.
[9] H. Fujita, V. T. Dau, K. Shimizu, R. Hatsuda, S. Sugiyama, E. Nagamori, *Biomedical Microdevices* 2011, *13*, 123.
[10] A. L. Baryshyan, L. J. Domigan, B. Hunt, B. A. Trimmer, D. L. Kaplan, *RSC advances* 2014, *4*, 39962.
[11] M. S. Sakar, D. Neal, T. Boudou, M. A. Borochin, Y. Li, R. Weiss, R. D. Kamm, C. S. Chen, H. H. Asada, *Lab on a Chip* 2012, *12*, 4976.
[12] J. Ramon-Azcon, S. Ahadian, M. Estili, X. B. Liang, S. Ostrovidov, H. Kaji, H. Shiku, M. Ramalingam, K. Nakajima, Y. Sakka, A. Khademhosseini, T. Matsue, *Advanced Materials* 2013, *25*, 4028.
[13] J. Ramon-Azcon, S. Ahadian, R. Obregon, G. Camci-Unal, S. Ostrovidov, V. Hosseini, H. Kaji, K. Ino, H. Shiku, A. Khademhosseini, T. Matsue, *Lab on a Chip* 2012, *12*, 2959.

[14] J. Visser, F. P. Melchels, J. E. Jeon, E. M. van Bussel, L. S. Kimpton, H. M. Byrne, W. J. Dhert, P. D. Dalton, D. W. Hutmacher, J. Malda, ***Nature Communications*** **2015,** ***6,*** **6933.**
[15] P. Bajaj, R. M. Schweller, A. Khademhosseini, J. L. West, R. Bashir, ***Annual review of biomedical engineering*** **2014,** ***16,*** **247.**
[16] Z.-M. Huang, Y. Z. Zhang, M. Kotaki, S. Ramakrishna, ***Composites Science and Technology*** **2003,** ***63,*** **2223.**
[17] C. L. Cummings, D. Gawlitta, R. M. Nerem, J. P. Stegemann, ***Biomaterials*** **2004,** ***25,*** **3699.**
[18] B. J. Kwee, D. J. Mooney, ***Current Opinion in Biotechnology*** **2017,** ***47,*** **16.**
[19] Cynthia M. Smith, Alice L. Stone, Robert L. Parkhill, Robert L. Stewart, Mark W. Simpkins, Anatoly M. Kachurin, William L. Warren, S. K. Williams, ***Tissue Engineering*** **2004,** ***10,*** **1566.**
[20] D. Loessner, C. Meinert, E. Kaemmerer, L. C. Martine, K. Yue, P. A. Levett, T. J. Klein, F. P. W. Melchels, A. Khademhosseini, D. W. Hutmacher, ***Nature Protocols*** **2016,** ***11,*** **727.**
[21] K. Yue, X. Li, K. Schrobback, A. Sheikhi, N. Annabi, J. Leijten, W. Zhang, Y. S. Zhang, D. W. Hutmacher, T. J. Klein, A. Khademhosseini, ***Biomaterials*** **2017,** ***139,*** **163.**
[22] Q. Gao, Y. He, J.-z. Fu, A. Liu, L. Ma, ***Biomaterials*** **2015,** ***61,*** **203.**
[23] M. Nakamura, S. Iwanaga, C. Henmi, K. Arai, Y. Nishiyama, ***Biofabrication*** **2010,** ***2,*** **014110.**
[24] L. Ouyang, C. B. Highley, C. B. Rodell, W. Sun, J. A. Burdick, ***ACS Biomaterials Science & Engineering*** **2016,** ***2,*** **1743.**
[25] C. B. Hutson, J. W. Nichol, H. Aubin, H. Bae, S. Yamanlar, S. Al-Haque, S. T. Koshy, A. Khademhosseini, ***Tissue Engineering. Part A*** **2011,** ***17,*** **1713.**
[26] L. E. Bertassoni, M. Cecconi, V. Manoharan, M. Nikkhah, J. Hjortnaes, A. L. Cristino, G. Barabaschi, D. Demarchi, M. R. Dokmeci, Y. Yang, A. Khademhosseini, ***Lab on a Chip*** **2014,** ***14,*** **2202.**
[27] W. Jia, P. S. Gungor-Ozkerim, Y. S. Zhang, K. Yue, K. Zhu, W. Liu, Q. Pi, B. Byambaa, M. R. Dokmeci, S. R. Shin, A. Khademhosseini, ***Biomaterials*** **2016,** ***106,*** **58.**
[28] O. Jeon, K. H. Bouhadir, J. M. Mansour, E. Alsberg, ***Biomaterials*** **2009,** ***30,*** **2724.**
[29] Yong X. Chen, Brian Cain, P. Soman, ***AIMS Materials Science*** **2017,** ***4,*** **363.**
[30] T. Kageyama, T. Osaki, J. Enomoto, D. Myasnikova, T. Nittami, T. Hozumi, T. Ito, J. Fukuda, ***ACS Biomaterials Science & Engineering*** **2016,** ***2,*** **1059.**
[31] C. M. Murphy, F. J. O'Brien, ***Cell Adhesion & Migration*** **2010,** ***4,*** **377.**
[32] N. Devi, T. K. Maji, ***AAPS PharmSciTech*** **2009,** ***10,*** **1412.**
[33] C. Zhuang, C. Shi, F. Tao, Y. Cui, ***International Journal of Biological Macromolecules*** **2017.**
[34] R. Reeves, A. Ribeiro, L. Lombardo, R. Boyer, J. B. Leach, ***Polymers*** **2010,** ***2,*** **252.**
[35] Y. Ke, G. S. Liu, J. H. Wang, W. Xue, C. Du, G. Wu, ***eXPRESS Polymer Letters*** **2014,** ***8,*** **841.**
[36] C. C. Ribeiro, C. C. Barrias, M. A. Barbosa, ***Biomaterials*** **2004,** ***25,*** **4363.**
[37] D. Wei, W. Xiao, J. Sun, M. Zhong, L. Guo, H. Fan, X. Zhang, ***Journal of Materials Chemistry B*** **2015,** ***3,*** **2753.**
[38] Hutanu D, Frishberg MD, Guo L, D. CC, ***Mod Chem appl*** **2014,** ***2,*** **132.**
[39] A. M. Kloxin, J. A. Benton, K. S. Anseth, ***Biomaterials*** **2010,** ***31,*** **1.**
[40] B. D. Fairbanks, M. P. Schwartz, C. N. Bowman, K. S. Anseth, ***Biomaterials*** **2009,** ***30,*** **6702.**

[41] H. Zimmermann, M. Hillgärtner, B. Manz, P. Feilen, F. Brunnenmeier, U. Leinfelder, M. Weber, H. Cramer, S. Schneider, C. Hendrich, F. Volke, U. Zimmermann, *Biomaterials* 2003, *24*, 2083.
[42] Y. S. Zhang, A. Arneri, S. Bersini, S.-R. Shin, K. Zhu, Z. Goli-Malekabadi, J. Aleman, C. Colosi, F. Busignani, V. Dell'Erba, C. Bishop, T. Shupe, D. Demarchi, M. Moretti, M. Rasponi, M. R. Dokmeci, A. Atala, A. Khademhosseini, *Biomaterials* 2016, *110*, 45.
[43] Y. Nishiyama, M. Nakamura, C. Henmi, K. Yamaguchi, S. Mochizuki, H. Nakagawa, K. Takiura, *Journal of Biomechanical Engineering* 2008, *131*, 035001.
[44] M. Costantini, S. Testa, E. Fornetti, A. Barbetta, M. Trombetta, S. M. Cannata, C. Gargioli, A. Rainer, *Frontiers in Bioengineering and Biotechnology* 2017, *5*.
[45] J. W. Nichol, S. T. Koshy, H. Bae, C. M. Hwang, S. Yamanlar, A. Khademhosseini, *Biomaterials* 2010, *31*, 5536.
[46] W. Liu, M. A. Heinrich, Y. Zhou, A. Akpek, N. Hu, X. Liu, X. Guan, Z. Zhong, X. Jin, A. Khademhosseini, Y. S. Zhang, *Advanced Healthcare Materials* 2017, *6*, 1601451.
[47] A. Béduer, T. Braschler, O. Peric, G. E. Fantner, S. Mosser, P. C. Fraering, S. Benchérif, D. J. Mooney, P. Renaud, *Advanced Healthcare Materials* 2015, *4*, 301.
[48] K. S. Lim, B. S. Schon, N. V. Mekhileri, G. C. J. Brown, C. M. Chia, S. Prabakar, G. J. Hooper, T. B. F. Woodfield, *ACS Biomaterials Science & Engineering* 2016, *2*, 1752.
[49] K. Y. Lee, D. J. Mooney, *Progress in polymer science* 2012, *37*, 106.
[50] J. Zhu, *Biomaterials* 2010, *31*, 4639.
[51] G. Camci-Unal, D. Cuttica, N. Annabi, D. Demarchi, A. Khademhosseini, *Biomacromolecules* 2013, *14*, 1085.
[52] A. Khodabukus, K. Baar, *Cells Tissues Organs* 2015, *202*, 159.
[53] M. P. Lutolf, P. M. Gilbert, H. M. Blau, *Nature* 2009, *462*, 433.
[54] H. Aubin, J. W. Nichol, C. B. Hutson, H. Bae, A. L. Sieminski, D. M. Cropek, P. Akhyari, A. Khademhosseini, *Biomaterials* 2010, *31*, 6941.
[55] A. J. Engler, M. A. Griffin, S. Sen, C. G. BÃ¶nnemann, H. L. Sweeney, D. E. Discher, *pathological implications for soft or stiff microenvironments* 2004, *166*, 877.
[56] A. J. Engler, S. Sen, H. L. Sweeney, D. E. Discher, *Cell* 2006, *126*, 677.
[57] K. Ralla, U. Sohling, D. Riechers, C. Kasper, F. Ruf, T. Scheper, *Bioprocess and Biosystems Engineering* 2010, *33*, 847.
[58] M.-C. Kim, Y. R. Silberberg, R. Abeyaratne, R. D. Kamm, H. H. Asada, *Proceedings of the National Academy of Sciences* 2018.
[59] O. Pertz, *Communicative & Integrative Biology* 2011, *4*, 436.
[60] J. F. Evers, D. Muench, C. Duch, *Developmental Biology* 2006, *297*, 214.
[61] J. Yin, M. Yan, Y. Wang, J. Fu, H. Suo, *ACS Applied Materials & Interfaces* 2018, *10*, 6849.
[62] C. S. Chen, M. Mrksich, S. Huang, G. M. Whitesides, D. E. Ingber, *Science* 1997, *276*, 1425.
[63] X. Zhao, Q. Lang, L. Yildirimer, Z. Y. Lin, W. Cui, N. Annabi, K. W. Ng, M. R. Dokmeci, A. M. Ghaemmaghami, A. Khademhosseini, *Advanced Healthcare Materials* 2016, *5*, 108.
[64] Y. Wu, Z. Wang, J. Y. H. Fuh, Y. S. Wong, W. Wang, E. S. Thian, *Journal of Materials Science: Materials in Medicine* 2016, *27*, 115.
[65] G. Agrawal, A. Aung, S. Varghese, *Lab on a Chip* 2017, *17*, 3447.
[66] P. Bajaj, B. Reddy, L. Millet, C. Wei, P. Zorlutuna, G. Bao, R. Bashir, *Integrative Biology* 2011, *3*, 897.